Article

Application of the Model of Spots for Inverse Problems

Nikolai A. Simonov [1]*

[1] Valiev Institute of Physics and Technology of Russian Academy of Sciences, Moscow, Russia; nsimonov@ftian.ru

* Correspondence: nsimonov@ftian.ru; Tel: +7-925-348-1997

Abstract: This article proposes application of a new mathematical model of *spots* for solving inverse problems using a learning method, which is similar to using the deep learning. In general, the spots represent vague figures in abstract "information spaces" or crisp figures with lack of information about their shapes and are adequate for representation human mental images and reasoning in Artificial Intelligence (AI). However, crisp figures are regarded as a special and limiting case of spots. A basic mathematical apparatus, basing on L4 numbers, has been developed for the representation and processing of qualitative information of elementary spatial relations between spots. Also, we defined L4 vectors, L4 matrices, and mathematical operations on them. Developed apparatus can be used in AI, in particular, for knowledge representation and for modeling qualitative reasoning and learning. Another application area is the solution of inverse problems by learning. For example, this can be applied to image reconstruction using ultrasound, X-ray, magnetic resonance, or radar scan data. The introduced apparatus was verified by solving problems of reconstruction of images, utilizing only qualitative data of its elementary relations with some scanning figures. This article also demonstrates application of spot-based inverse Radon algorithm for binary image reconstruction.

Keywords: inverse problems; image reconstruction; vague figures; mental images; Artificial Intelligence

1. Introduction

Imaging based on the scan data of the object under study and the processing of scattered signals received by sensors refers to inverse problems. Relevant direct problems are the modeling of wave signals scattered from a known distribution of material properties within an object. [1,2]. In particular, medical devices that provide such imaging are CT, MRI, microwave tomography, electrical resistance and capacitance tomography, ultrasound imaging, and others [3]. There are other areas of application for such image reconstruction, including radar, ground-penetrating radar and through-the wall radar imaging. Geophysics also uses visualization obtained by sounding the earth with the help of sound or electrical impulses, etc. [1,4]. Imaging in all these areas, with the exception of MRI, is associated with the solution of *inverse scattering* problems in one or another approximation [5].

The fundamental point here is that practically it is impossible to obtain a mathematically exact solution of the inverse problem, however, it is possible to approximately reconstruct an image with a finite spatial resolution. Generally speaking, inverse problems relate to ill-posed mathematical problems, and such property can be explained by a lack of information for an exact solution due to the noise and the finite amount of the sensor signals. Therefore, approximate solution methods are used that utilize regularization, filtering, interpolation, and other approaches [3]. For example, this applies to CT, MRI, ultrasound, as well as to studies on microwave tomography [6–10].

Note that conventional approximate reconstruction methods such as filtered back-projection in CT or simple inverse FFT in MRI are not always adequate and may lead to artifacts. Therefore, new methods based on appropriate models have been developed that

 doi:10.20944/preprints202212.0423.v1

more strictly take into account the physics of objects and the real properties of sensors [11–14]. In a rigorous formulation, the inverse problem is considered as a nonlinear optimization with the regularization to find the minimum of the residual error (the norm of deviation of the received and calculated sensor data). Its solution is sought by the iterative method, where the direct problem is solved and the current residual error is calculated at each iteration step [5]. This rigorous approach is especially relevant for microwave tomography, where one has to solve the nonlinear inverse problem of electromagnetic scattering. Unfortunately, using simple and approximate reconstruction methods is inadequate here, since microwave scanning of a part of the body is performed in the near-field area of antennas, and also multi-pass scattering effects are significant [6–10]. A big issue is the fact that iterative solutions, especially for electromagnetic scattering, require a long execution time and consume large computer resources [7].

In recent years, much attention has been paid to solving nonlinear inverse problems using artificial intelligence (AI) approach, applying neural networks of deep learning [15–21]. The idea of this method is that if the neural network is successfully trained on examples, then when new scattering signals are fed to the input of the network, the trained system can create the desired image directly on the basis of the acquired knowledge, without solving the complex inverse scattering problem. Another area of application of learning neural networks is their use for image recognition, classification and segmentation [22–24].

However, many authors point out the disadvantage of the traditional model of artificial neurons in neural networks, which consists in excessive computational accuracy and an excessive number of adjustable system parameters. [25]. Indeed, the apparatus of 32-bit floating-point numbers is utilized in learning algorithms for input signals, weight coefficients, activation and loss functions. Then a lot of operations during the training process leads to large consumption of computer resources and execution time. For example, the training time for image recognition (which is a simple task for humans) can be on the order of several weeks even in high-performance systems [26]. Obviously, it cannot be implemented on compact devices with limited resources and limited power consumption.

Therefore, intensive research is currently underway to develop algorithms using reduced bit width of numbers: 8 bits, 4 bits, 2 bits, and even 1 bit. This provides a rough approximation for all the network parameters and such optimized neural networks are called binarized [25]. It should be noted that deep learning networks, which are used, for example, for image recognition task, operate with 32-bit numbers, while it is obvious that high accuracy is not required for such an image classification [26].

A new mathematical model of spots is proposed in [27,28] for representation and processing incomplete, inaccurate or qualitative information. In particular, it allows to create algorithms of a new type for AI and build neuromorphic systems, which operates in the way that is close to the human thinking. Instead of real numbers, the proposed model introduces logical L4 numbers, L4 vectors and L4 matrices. The spot model allows one to represent mental images and semantic content of information, as well as make classification and fragmentation. A new approach for machine learning has also been suggested, which applicable for solving inverse problems. In addition, a new architecture of neural networks is proposed, consisting of layers that are modeled by L4 matrices, input and output data are L4 vectors, and weight coefficients are L4 numbers.

Thus, in the spots model, information representation, storage and processing are carried out using 4-bit logical L4 numbers, rather than 32-bit numbers that can significantly reduce the consumption of machine resources. Behind, developed learning algorithm does not use such complex calculations and iterations as in the backpropagation algorithm for learning from examples [29].

The main idea of the theory of spots is that the synthesis of a large amount of even insignificant information allows one to extract detailed and even quantitative information about the object of interest. Since the ill-posedness of inverse problems leads to indefinite, fuzzy, and ambiguous solutions, the application of the spot apparatus seems to be quite adequate.

 doi:10.20944/preprints202212.0423.v1

The proposed theory turned out to be ideologically close to the research areas of mereotopology and qualitative geometry [30–48], the idea of which was laid down by Whitehead in 1929 [30]. On the other hand, basic ideas of the spots model are also close to the rough set theory [49–56], the formal concept analysis [53,57–59], and the fuzzy set theory [60], including fuzzy geometry [61,62]. Moreover, the suggested concept is in a good agreement with the ideology of the granular computing [63–69].

Instead of points, mereotopology uses regions of space as the primitive spatial entity, and utilizes qualitative information of their relations. Among other areas, it has been applied to geographical information science, and image analysis [38]. One of the important fields of mereotopology is region connection calculus (RCC) [34,35], which has two variants. RCC-8 defines eight relations between regions, including overlapping, disconnection, external connection, and connections (touch) of the region's boundaries. Bennett [42], as well as Jonsson and Drakengren [43] considered a shortened version of these relations – RCC-5, which does not consider the boundaries connection. A feature of RCC-5 is the uncertainty of boundaries, since here it is impossible to distinguish internal points from boundary ones.

Although most authors considered spatial relations as logical values, Egenhofer et al. [44, 45] encoded them in form of logical tables. Namely, they introduced the concepts of 4-intersection [44] and 9-intersection [45] matrixes, which are logical matrices that encode the spatial relations between spatial regions. Notice that these matrixes are similar but differ from the L4 numbers proposed in [27,28] because authors of [44, 45] consider also relations with the boundaries. Clementini et al. [46] generalized 9-intersection matrixes, replacing intersections for the crisp boundary with the intersections for broad boundaries. Stell [47] also considered the way of representation for spatial relations using 3x1 logical vectors created on the base of notions *part* and *compliment* only. Finally, Butenkov [48] introduced 2x2 logic tables for Cartesian granules, which are equivalent to L4 numbers for spots, and applied them in data mining algorithms.

The rough set theory suggested by Zdzisław Pawlak [49,50] is a mathematical approach for the representation of the vagueness. One of the main advantages of the rough set approach is the fact that it does not need any preliminary or additional information about data – like probability in statistics, or membership in the fuzzy set theory. This theory regards sets with incomplete information that does not allow to distinguish elements in some their subsets, which are called granules. Pawlak's theory introduced such notions as the lower and upper approximations of rough set, the boundary region and the membership function for elements, which is similar to that for the fuzzy sets.

A general formulation and consideration of granules, including the problem of information granulation, which was later called the concept of granular computing, were firstly carried out by Zadeh in [63]. His definition of granules: "the information may be said to be granular in the sense that the data points within a granule have to be dealt with as a whole rather than individually" corresponds to the equivalence classes of the universe. Zadeh regards both crisp and fuzzy granules and "considers granular computing as a basis for computing with words, i.e., computation with information described in natural language" [64]. The elements of a granule are indiscernible that "depends on available knowledge" [66]. The importance of the application of granulation and granular computing relates to the fact that such approximation leads to simplification in solving practical problems.

The graph is a mathematical model convenient for the representation of the structure of links (labeled edges) between elements (nodes or vertexes) of the system under study [70]. Nowadays, networks based on the application of graph theory are widely used in AI. For example, the apparatus of graphs is well suited for the analysis and processing of digital images in the digital geometry [71] and for the analysis and metrics of the structure of the physical connection of brain neurons [72]. On the other hand, graph theory is actively used to model semantic networks, which are used in the knowledge base, which are called knowledge graphs [73–77]. Note that, unlike spots, the graph is only an abstraction for a structure of the relations between the entities, rather than is a spatial object. However,

Preprints (www.preprints.org) | NOT PEER-REVIEWED | Posted: 22 December 2022 doi:10.20944/preprints202212.0423.v1

recent works utilize graph's embedding in some continuous space for reduce the dimention of the graph when processing its data [75–77].

Despite the ideological closeness to these theories, the proposed model of spots has a significantly different nature, since spots are not defined on the base of sets or fuzzy sets and spot's elements do not defined. Instead, a spot can have a structure inside that is determined from spatial relations with other spots. Having elementary spatial properties, spots combine the concepts of discreteness and continuity, while graphs are discrete mathematical objects. Generally, the presence of similar mathematical models allows us to apply some approaches and ideas from them.

2. Definition of spots and the apparatus of L4 numbers

Spots are mathematical objects with elementary spatial properties, for which their inner region, outer region (environment) and a logical connection between these regions for any two spots are defined. The logical connection ab of two spots a, b is determined by two axioms [31], [35]

$$\forall a, aa = 1 \text{ (logical)} \tag{1}$$

$$\forall a \forall b, ab = ba \tag{2}$$

Environments $\tilde{a}, \tilde{b}$ of spots a, b are also considered to be spots, therefore, a logical connection is also defined for them, satisfying the axioms (1) and (2). Axiomatically, we regard spots do not connect their environments, that is

$$a\tilde{a} = 0, \qquad b\tilde{b} = 0 \tag{3}$$

In general, "shape" of spots and the properties of their environment, like dimension and curvature of space, are not predetermined, but can be evaluated from qualitative information about their elementary spatial relations (ER) to other spots, such as separation, intersection, inclusion, indistinguishability, etc. We consider crisp geometric figures as a special limiting case of spots.

Note that the connection can be defined not only for the case of the existence of a common region of space for two spots, but also in a more general sense. For example, two geometric figures can be considered indistinguishable if they can be precise coincided by a rigid movement. In general, any spot mapping can be defined on the base of ER.

2.1. Definition of L4 numbers

The elementary relations can be formalized using logical L4 numbers [27]. For spots a, b and their environments $\tilde{a}$, $\tilde{b}$ the L4 number $\langle a|b\rangle$ is defined as a table

$$\langle a|b\rangle = \begin{bmatrix} ab & a\tilde{b} \\ \tilde{a}b & \tilde{a}\tilde{b} \end{bmatrix} \tag{4}$$

where ab, $a\tilde{b}\ldots$ denote the logical connections. Such L4 numbers, in general, permits to distinguish 16 different ER between spots. Examples of the ER and their corresponding L4 numbers are shown in Table 1. We call these spatial relations as elementary relations because they carry lowest-level qualitative information about spots. However, a large amount of such qualitative data allows extract higher-level qualitative information and even numerical information.

The mathematical apparatus of the spot model is based on the L4 numbers, rather than on real numbers. As far as the basis of this apparatus is described in more detail in the previous works [27,28], here we will briefly outline the main content and reveal the meanings of the concepts introduced there.

Table 1. Some ER of spots.

Elementary relations	L4 number

Preprints (www.preprints.org) | NOT PEER-REVIEWED | Posted: 22 December 2022 doi:10.20944/preprints202212.0423.v1

intersection, $a >< b$	$\begin{bmatrix}1 & 1\\ 1 & 1\end{bmatrix}$
separation, $a <> b$	$\begin{bmatrix}0 & 1\\ 1 & 1\end{bmatrix}$
inclusion (more), $a > b$	$\begin{bmatrix}1 & 1\\ 0 & 1\end{bmatrix}$
inclusion (less), $a < b$	$\begin{bmatrix}1 & 0\\ 1 & 1\end{bmatrix}$
indiscernibility, $a \approx b$	$\begin{bmatrix}1 & 0\\ 0 & 1\end{bmatrix}$

In [27,28], the basis of spots is defined as a collection of "known" spots that can be in some mutual ER. The representation of a spot by their ER on the basis spots is a mapping or imaging of the spot on this basis. Note that the system of basis spots is analogous to the numerical basis functions, and the orthogonality of the basis functions is analogous to the separated basis spots, which we call *orthogonal* spots. Let's call the collection of spots with a certain ER between them the structure of spots. The structure of the basis spots included in a spot a will also be called the *structure* of the spot a.

Note that the spot mapping is generally similar to the concept of projection for crisp figures. Consequently, the spot is analogous to some volumetric object, which is determined by its projections on different planes. Hence, one can improve knowledge about structure of the spot by fusion its mappings on different bases into a "volumetric" image.

Let us define operations union $\vee$ and the intersection $\wedge$ for the spots, which permits to create new spots. We suggest the following definitions, which are similar but different from those of the set theory:

$$\begin{aligned} c = a \vee b &\leftrightarrow \forall x\,(cx = ax + bx)\\ \mathrm{d} = a \wedge b &\leftrightarrow \forall x\left(\tilde{d}x = \tilde{a}x + \tilde{b}x\right)\end{aligned} \tag{5}$$

Here symbol + denotes the logical disjunction operation. Note that, in contrast to the sets, (5) does not define the images of spots c, d absolutely determined, because they depend on spots basis $\{x_i\}$. Following the equality $c\tilde{c} = 0$, see (3), it is possible, for example, to derive the following equations from (5):

$$c = \bigvee_i x_i\,, \qquad x_i : \left(\tilde{a}x_i + \tilde{b}x_i = 0\right) \tag{6}$$

The definitions (5) permit to derive simple properties for zero spots $\emptyset$:

$$a \vee \emptyset = a,\ a \wedge \emptyset = \emptyset \tag{7}$$

and also express intersection parts A, B, C, and D of spots a and b in Figure 1, using the operation $\wedge$:

$$A = a \wedge \tilde{b},\ B = \tilde{a} \wedge b,\ C = a \wedge b,\ D = \tilde{a} \wedge \tilde{b} \tag{8}$$

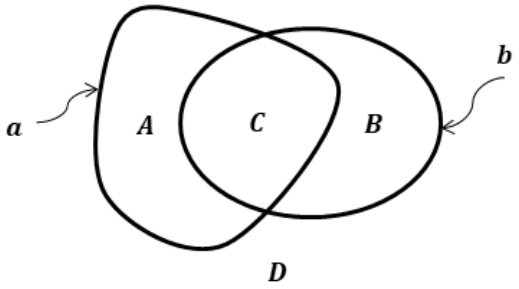

Figure 1: Euler-Venn diagram for the elementary relations between spots.

2.2. Definition and geometric meaning of L4 vectors and L4 matrices

Preprints (www.preprints.org) | NOT PEER-REVIEWED | Posted: 22 December 2022 doi:10.20944/preprints202212.0423.v1

As mentioned earlier, information about any spot can be defined as its mapping on some basis. Then it can be encoded as a vector with coordinates corresponding to its ER with basis spots. Such a vector of L4 numbers is called an L4 vector. For example, the L4 column vector $\boldsymbol{a}_X$ [27] of the spot a, represented on the base $X = \{x_i\}$, is

$$\boldsymbol{a}_X \equiv [\langle a|x_1\rangle;\ \langle a|x_2\rangle;\ \dots;\ \langle a|x_n\rangle] \tag{9}$$

where n is a number of spots in the basis X, is similar to a numerical vector but its elements are L4 numbers. Note that mapping (9) is also similar to projection of a 3D body on some plane, which, obviously, can only carry partial information about the body.

Papers [27,28] introduce idealized concept of *atomic* basis, which is a collection of atomic spots, which do not intersect each other and other spots. Note that the atomic spots are similar to points, pixels, voxels, or elements of sets. Another useful notion is *orthogonal* spots, for which their mutual ER are separation. For example, intersection parts of spots are orthogonal and can be regard as some approximation for the atomic basis.

The L4 matrix $\mathbf{A} = \langle Y|X\rangle$ defines ER between the spots of two bases, $X = \{x_i\}$ and $Y = \{y_j\}$ and formalizes the mapping from X basis to Y basis:

$$\langle Y|X\rangle \equiv \left[\langle y_j|x_i\rangle\right] = [(\boldsymbol{y}_1)_X;\ (\boldsymbol{y}_2)_X;\ \dots;\ (\boldsymbol{y}_n)_X] \tag{10}$$

Here $(\boldsymbol{y}_j)_X$ are row L4 vectors of spot y_j, represented on the basis X. Note that the L4 matrix can be used to transform the L4 vector from one to another basis [27] that is similar to the mapping function in topology and geometry. Formally, it can be represented in the form of

$$\boldsymbol{a}_Y = \langle Y|X\rangle\, \boldsymbol{a}_X$$

however, there is no simple solution for defining rules for such a product, and we will address this issue in the next section. The exception is the special case of L4-matrix, which we call the indistinguishability matrix that is similar to the numerical identity matrix. The indiscernibility matrix $\mathbf{I}$ has diagonal elements corresponded to the indiscernibility and all other elements – to separation. Then multiplication L4 matrix $\mathbf{I}$ and any L4 vector $\boldsymbol{a}$ corresponds to an identity transformation:

$$\boldsymbol{a} = \mathbf{I}\,\boldsymbol{a}$$

There is a special case when all the spots of two bases are separated that is analogous to orthogonal coordinates in geometry. It is obvious that in this case it is impossible to obtain a mapping transformation using the product of an L4 matrix and L4 vector, and it is necessary to obtain additional independent data.

2.3. Multiplication Rules for L4 Vectors and L4 Matrixes

First, consider the simplest case of an atomic basis $A = \{u_i\}$, where basis spots are orthogonal and do not intersect other spots [27,28]. For it, one can define an ER $\langle a|b\rangle_A$ between the spots a and b with respect to the basis A and the "scalar" product of vectors $(\boldsymbol{a}_A, \boldsymbol{b}_A)$ according to the rule

$$\langle a|b\rangle_A = (\boldsymbol{a}_A, \boldsymbol{b}_A) = \begin{bmatrix} \sum_{i=1}^{n} au_i \cdot bu_i & \sum_{i=1}^{n} au_i \cdot \tilde{b}u_i \\ \sum_{i=1}^{n} \tilde{a}u_i \cdot bu_i & \sum_{i=1}^{n} \tilde{a}u_i \cdot \tilde{b}u_i \end{bmatrix} \tag{11}$$

where the symbol "·" denotes a logical conjunction. We will apply the same rule for an orthogonal basis $U = \{u_i\}$, consisting of separated spots.

Let us regard a spot a, basis $B = \{b_i\}$ and an atomic basis $A = \{u_i\}$. We suppose that a and all b_i spots can be mapped on the atomic basis A. Then the rule for product of L4 matrix $\langle B|A\rangle$ (10) and L4 vector $\boldsymbol{a}_A$ (9) can be defined as following:

Preprints (www.preprints.org) | NOT PEER-REVIEWED | Posted: 22 December 2022 doi:10.20944/preprints202212.0423.v1

$$\boldsymbol{a}_B = \langle B|A\rangle\, \boldsymbol{a}_A = [\langle a|b_i\rangle_A] \tag{12}$$

where L4 number $\langle a|b_i\rangle_A$ is defined in (11). Note that equation (12) defines transformation of the mapping of the spot a from basis A to basis B.

For an arbitrary basis $X = \{x_i\}$, for which spots x_i can be intersected, the definition of $\langle a|b\rangle_X$ is more complicated. First, let us consider the orthogonal basis $U = \{u_i\}$ of all intersections of the spots in X and find the vectors $\boldsymbol{a}_U = [\langle a|u_k\rangle]$ and $\boldsymbol{b}_U = [\langle b|u_k\rangle]$ on the basis U. Then we define the following equality for calculation $\langle a|b\rangle_X$:

$$\langle a|b\rangle_X = (\boldsymbol{a}_U, \boldsymbol{b}_U) = \langle a|b\rangle_U$$

and apply the rule (11). We define the vectors $\boldsymbol{a}_U$ and $\boldsymbol{b}_U$ using the following matrix equations:

$$\begin{aligned} \boldsymbol{a}_U &= \langle U|X\rangle\, \boldsymbol{a}_X, \\ \boldsymbol{b}_U &= \langle U|X\rangle\, \boldsymbol{b}_X \end{aligned} \tag{13}$$

where $\langle U|X\rangle$ is the L4 matrix that consist on $\langle u_i|x_j\rangle$ elements and is used for mapping vectors from basis X to basis U.

To determine the transformation rule for (13), we first apply a convenient method of numbering the intersections $\{u_k\}$ of spots $\{x_i\}$, using a binary code. Namely, generalizing (8), each u_k can be defined in terms of the spots x_i or $\tilde{x}_j$ connected by operators $\wedge$. For example, the binary index $k = 101\ldots0_2$ corresponds to the following spot u_k [28]:

$$u_k = x_1 \wedge \tilde{x}_2 \wedge x_3 \ldots \wedge \tilde{x}_n \tag{14}$$

ER $\langle a|u_k\rangle$ for any spot a and for u_k (14) can be found using the following approximate equation [28]

$$\langle a|u_k\rangle = \begin{bmatrix} ax_1 \cdot a\tilde{x}_2 \cdot \ldots \cdot a\tilde{x}_n & a\tilde{x}_1 + ax_2 + \cdots + ax_n \\ \tilde{a}x_1 \cdot \tilde{a}\tilde{x}_2 \cdot \ldots \cdot \tilde{a}\tilde{x}_n & \tilde{a}\tilde{x}_1 + \tilde{a}x_2 + \cdots + \tilde{a}x_n \end{bmatrix} \tag{15}$$

which defines the rule for the product $\langle U|X\rangle\, \boldsymbol{a}_X$ in (13). A similar equation can be written for the spot b to determine the product $\langle U|X\rangle\, \boldsymbol{b}_X$ in (13). Equation (15) was tested in [28] when solving the problem of reconstruction the shape of plane figures, processing its ER data with known figures [28, fig. 4–6]. It turned out that (15) gives uncertainty in the form of a blurred boundary. To eliminate it, we applied additional rules, correcting ER $\langle a|u_k\rangle$ in (15):

$$\begin{aligned} &\text{if } \{\forall x_j : ax_j = 0,\ u_k x_j = 0\}\ then\ a > u_k \\ &\text{if } \{\forall x_j : \tilde{a}x_j = 0,\ u_k x_j = 0\}\ then\ a <> u_k \end{aligned} \tag{16}$$

where the symbols $<>$ and $>$ denote the separation and inclusion (more) relations, respectively (see Table 1).

Equations (15) and (16) help to determine the general rule for multiplying an arbitrary L4 vector $\boldsymbol{a}_X$ and an L4 matrix $\mathbf{A} = \langle Y|X\rangle$ defined on the basises $X = \{x_i\}$ and $Y = \{y_j\}$. We can write this rule in the following form:

$$\boldsymbol{a}_Y = \langle Y|X\rangle\, \boldsymbol{a}_X = \langle Y|V\rangle \cdot \langle V|W\rangle \cdot \langle W|U\rangle \cdot \langle U|X\rangle\, \boldsymbol{a}_X \tag{17}$$

Here the basis $U = \{u_i\}$ consists of the intersections of the points x_i, $V = \{v_i\}$ is the basis of the intersections of the spots $\{y_j\}$, and $W = \{w_i\}$ is the basis of the intersections of the spots of U and V basises. Note that equation (17) should be considered as a series of transformations from one basis to another, namely

$$\boldsymbol{a}_U = \langle U|X\rangle\, \boldsymbol{a}_X,\ \boldsymbol{a}_W = \langle W|U\rangle\, \boldsymbol{a}_U,\ \boldsymbol{a}_V = \langle V|W\rangle\, \boldsymbol{a}_W,\ \boldsymbol{a}_Y = \langle Y|V\rangle\, \boldsymbol{a}_V \tag{18}$$

Preprints (www.preprints.org) | NOT PEER-REVIEWED | Posted: 22 December 2022 doi:10.20944/preprints202212.0423.v1

Product $\langle U|X\rangle\,\boldsymbol{a}_X$ can be calculated, using (15) and (16), but the vectors $\langle V|W\rangle\,\boldsymbol{a}_W$ and $\langle Y|V\rangle\,\boldsymbol{a}_V$ – using (11), (12), regarding V, W as atomic basises. Finally, let us use the following natural rule for calculation the product $\langle W|U\rangle\,\boldsymbol{a}_U$:

$$\text{if } w_k < u_i \;\rightarrow \langle a|w_k\rangle = \langle a|u_i\rangle \tag{19}$$

where symbols $<$ denotes relation inclusion (less) (see Table 1). Note that the rule (19) is also approximate.

3. General Approach to Inverse Problems and Learning Using L4 Matrices

3.1. Solution of Inverse Problems

It follows from the definition of L4 matrices $\langle Y|X\rangle$ (10) that its inverse matrix $\langle X|Y\rangle$ is equal to

$$\langle Y|X\rangle^{-1} \equiv \langle X|Y\rangle = \left[\langle x_i|y_j\rangle\right] \tag{20}$$

and hence it must always exist and be equal to the transposed matrix $\langle Y|X\rangle$ with an additional transposed its elements (L4 numbers). Therefore, as it following from (17) and (20), formally the solution of the equation $\boldsymbol{a}_Y = \langle Y|X\rangle\,\boldsymbol{a}_X$ can be represented as

$$\widehat{\boldsymbol{a}}_X = \langle X|Y\rangle\,\boldsymbol{a}_Y = \langle X|U\rangle\cdot\langle U|W\rangle\cdot\langle W|V\rangle\cdot\langle V|Y\rangle\,\boldsymbol{a}_Y \tag{21}$$

where, as in (17), the basis U consists on intersections of the spots in X, the basis V – intersections of the spots in Y and W – intersections of the spots of U and V basis. Considering that equations (15) - (17) and (19) are approximate, we can conclude that in the general case, the inverse solution (21) is also approximate:

$$\boldsymbol{a}_X \cong \widehat{\boldsymbol{a}}_X = \langle Y|X\rangle^{-1}\,\boldsymbol{a}_Y$$

3.2. Solving inverse problems using L4 matrices by learning method

As mentioned in the introduction, practical application of solving inverse problems, especially electromagnetic inverse scattering, requires large amount of computing time and resources. Alternative approaches involve the use of the neural networks to train a solving system, which, after training, can make an inverse solution for new measured data. In the spots model, this has an analogy with the situation when the matrix $\mathbf{A} = \langle Y|X\rangle$ in (17) is unknown and it is wanted to be determined on training examples. It is necessary to evaluate an unknown L4 matrix $\mathbf{A}$ on the base of a set of training examples $\{\boldsymbol{x}_i, \boldsymbol{y}_i\}$, using the equality

$$\boldsymbol{y}_i = \mathbf{A}\,\boldsymbol{x}_i \tag{22}$$

Let us regard $\boldsymbol{x}_i, \boldsymbol{y}_i$ as L4 vectors for spots x_i and y_i that form the basises $X = \{x_i\}$ and $Y = \{y_i\}$ of the training data. Then we can compose L4 matrix $\langle Y|X\rangle$ and the matrix $\mathbf{A}$ in (22) can be represented as:

$$\mathbf{A} = \langle B_Y|Y\rangle\cdot\langle Y|X\rangle\cdot\langle X|B_X\rangle \tag{23}$$

where B_X and B_Y are atomic basises, which represent L4 vectors $\boldsymbol{x}_i$ and $\boldsymbol{y}_i$, correspondingly. Obviously, for testing set the data matrix $\langle Y|X\rangle$ is equal to the indistinguishability matrix $\mathbf{I}$. Note that equation (23) is a schematic interpretation of the learning process [29].

Let us consider application of the learning system to obtain the inverse solution of the equation (23)

$$\boldsymbol{b} = \langle B_Y|Y\rangle\cdot\langle Y|X\rangle\cdot\langle X|B_X\rangle\,\boldsymbol{a}$$

To do this, we can use the transformation of the matrix $\mathbf{A}$ (23), similar to (21), to represent the inverse solution in the following general form:

Preprints (www.preprints.org) | NOT PEER-REVIEWED | Posted: 22 December 2022 doi:10.20944/preprints202212.0423.v1

$$\boldsymbol{a} \cong \hat{\boldsymbol{a}} = \langle B_X|X\rangle \cdot \langle X|Y\rangle \cdot \langle Y|B_Y\rangle\, \boldsymbol{b} \tag{24}$$

We should especially consider the case when input data $\boldsymbol{c}$ and/or output data $\boldsymbol{d}$ are numeric. Then, instead of matrixes $\langle Y|B_Y\rangle$ or $\langle B_X|X\rangle$ in (24) we have to apply corresponding operators $\boldsymbol{B}_X$ and $\boldsymbol{B}_Y$ that transforms L4 data to numerical data or vice versa. Then the forward problem has the form of

$$\boldsymbol{d} = \boldsymbol{B}_Y(\boldsymbol{c}_Y) \cdot \langle Y|X\rangle \cdot \boldsymbol{B}_X(\boldsymbol{c})$$

and its inverse solution instead of (24) can be represented in the following form:

$$\boldsymbol{c} \cong \boldsymbol{B}_X^{-1}(\boldsymbol{d}_X) \cdot \langle X|Y\rangle \cdot \boldsymbol{B}_Y^{-1}(\boldsymbol{d}) \tag{25}$$

where $\boldsymbol{B}_X^{-1}$ and $\boldsymbol{B}_Y^{-1}$ are the inverse operators.

3.3. Image Reconstruction by Processing Qualitative Data

Although the proposed theory is developed for spots, which in general correspond to vague figures, it is convenient to verify its mathematical apparatus on crisp figures, which are the limiting case of spots. Let us consider the figure under test as a conditionally unknown spot, and the figures, which are used for mapping this spot (or "sampling") as known basis of spots [28]. More specific, we consider the shape reconstruction of a crisp plane figure, utilizing the only qualitative information of its ER with the basis figures without addition details about these relations. However, it is possible to infinitely refine the reconstructed shape of the unknown figure by increasing the number of samplings and processing all the ER data. It may seem surprising, but it is theoretically possible to reconstruct the shape of an object with absolute precision. This is a consequence of the following theorem.

Theorem 1. *In order for two figures to be pointwise equal, it is necessary and sufficient that their elementary relations with any other figure of finite size be the same.*

Proof. Necessity. As can be seen from the diagram in Figure 2, the condition of equality of figures a and b is equivalent of equality of both their intersection parts A and B to the zero figure $\emptyset$. Let us suppose there is a figure c that has different ER with a and b, i.e., different connection values with these figures. For example, $ac = 0$, $bc = 1$ (Figure 2). Then $\{\exists E = b \wedge c: aE = 0\} \rightarrow E \subset B = \tilde{a} \wedge b \rightarrow B \neq \emptyset$. Therefore, $a \neq b$, which proves the necessity condition.

Sufficiency. Let us prove by contradiction. Assume that for two figures a and b their ER is equal with any finite figure, but $a \neq b$. Then, $(A \neq \emptyset) \vee (B \neq \emptyset)$ (see Figure 2). If, for example, $B \neq \emptyset$, then $\exists c: \{ac = 0, Bc = 1\} \rightarrow bc = 1$ that contradicts the condition of equality ER with any finite figure. Therefore, the assumption $a \neq b$ is false, which proves the sufficiency condition. □

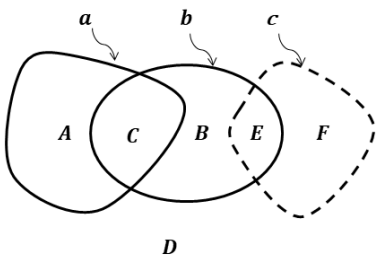

Figure 2: Euler-Venn diagram for ER between figures a, b and c.

It follows from Theorem 1 that all information about the shape of each figure is contained in the infinite set of its ER with all other figures of finite size. Therefore, in principle, it is possible to reconstruct this shape using such qualitative information. However, due to the incomplete, finite amount of ER data, figure shape reconstruction can only be

Preprints (www.preprints.org) | NOT PEER-REVIEWED | Posted: 22 December 2022 doi:10.20944/preprints202212.0423.v1

approximate. This corresponds to the fact that the result of such a reconstruction corresponds to a blurry figure, that is, to a spot.

Note that the shape reconstruction by processing qualitative data refers to inverse problems. Indeed, its forward problems can be formulated as

$$\boldsymbol{a}_X = \langle X|P\rangle\, \boldsymbol{a}_P \tag{26}$$

where P is a basis of atomic spots – pixels or voxels, $X = \{x_i\}$ is a basis of scanning figures for testing, $\boldsymbol{a}_X$ – L4 vector of ER data for the reconstruction of figure under test $\boldsymbol{a}_P$. Following to (21), the reconstructed figure $\widehat{\boldsymbol{a}}_P$ is the inverse solution of (26) that, similar to (21), can be represented in the form of equation

$$\widehat{\boldsymbol{a}}_P = \langle P|X\rangle\, \boldsymbol{a}_X = \langle P|U\rangle \cdot \langle U|X\rangle\, \boldsymbol{a}_X \tag{27}$$

where U is a basis of intersections of spots $\{x_i\}$. The mapping $\boldsymbol{a}_U = \langle U|X\rangle\, \boldsymbol{a}_X$ can be found using (15) and (16).

3.4. Inverse Radon algorithm for binary figures

Let us consider scanning figures - squares as the basis $X = \{x_i\}$ and use the calculated sinograms (projections) S of these squares as training data, which we will assign to the basis $Y = \{y_i\}$. As before, $\{x_i, y_i\}$ will be considered as training data for the learning system, and we will determine an algorithm for the inverse solution by learning.

Obviously, the forward problem is the Radon transform that can be written in the form of

$$\boldsymbol{s} = \boldsymbol{R}(\boldsymbol{a}_P) \tag{28}$$

where P is basis of pixels, $\boldsymbol{R}$ is the Radon transform operator, $\boldsymbol{s}$ is the sinograms of the $\boldsymbol{a}_P$ image. Following (25), the inverse Radon solution of (28) can be represented as

$$\widehat{\boldsymbol{a}}_P = \langle P|U\rangle \cdot \langle U|X\rangle \cdot \langle X|Y\rangle \cdot \boldsymbol{B}_Y^{-1}(\boldsymbol{s}) \tag{29}$$

where U is the basis of intersections of $\{x_i\}$. Note, the operator $\boldsymbol{B}_Y^{-1}$ depends on the training sinograms data S and matrix $\langle Y|X\rangle$ is the indiscernibility matrix $\mathbf{I}$ for the solving by learning methods, as it was mentioned before. Therefore,

$$\widehat{\boldsymbol{a}}_P = \langle P|U\rangle \cdot \langle U|X\rangle\, \boldsymbol{a}_X\,; \quad \boldsymbol{a}_X = \boldsymbol{a}_Y = \boldsymbol{B}_Y^{-1}(\boldsymbol{s}) \tag{30}$$

Let us found rules for calculation $\boldsymbol{a}_Y$ (30), defining such ER between sinograms that are presented in Figure 3. Here small spiking sinograms (continue lines) correspond to relatively small basis squares x_i and oval type sinograms (dashed lines) correspond to ellipse figure $\boldsymbol{a}_P$ (see Subsection 4.3).

(**a**) (**b**) (**c**)

Figure 3. ER between sinograms of an ellipse and a basis square. (**a**) Separation; (**b**) Inclusion; (**c**) Intersection.

The main idea of suggesting algorithm is that if basis figure x_i has such ER with the figure under test a as separation or intersection, then there are projection angles for which their sinograms are separated or intersected. But if x_i is included in a then all their sinograms has ER inclusion as well. Hence, we can define the following rules for ER of projections $s_X(i,j,k)$ and $s_a(i,j,k)$, which are converted to *logical values*:

Preprints (www.preprints.org) | NOT PEER-REVIEWED | Posted: 22 December 2022 doi:10.20944/preprints202212.0423.v1

$$\begin{aligned} \boldsymbol{a}_X(i) &= \langle a|x_i\rangle = \begin{bmatrix} ax_i & 1 \\ \tilde{a}x_i & 1 \end{bmatrix} \\ ax_i &= \sum_k \sum_j s_a(i,j,k) \cdot s_X(i,j,k) \\ \tilde{a}x_i &= \sum_k \sum_j \neg s_a(i,j,k) \cdot s_X(i,j,k) \end{aligned} \tag{31}$$

Here $\neg$ is the logical negation, i-index corresponds to that of x_i square, j-index corresponds to the projection coordinate $\xi(j)$ and k-index corresponds to the projection angle $\alpha_0(k)$ [2, Sec. 8.7.3]. Using (30) and (31) we get spot-based inverse Radon algorithm for the reconstruction of binary images.

4. Results of Image Reconstruction

4.1. Reconstruction of Binary Images

To illustrate the suggested theory, MATLAB programs were written that provide processing of ER data between the figure under test and basis spots (crisp figures) x_i, using (27) and algorithm (15), (16). To obtain better resolution, we utilize quite tight distribution of the basis spots that makes the intersections u_k (14) to be relatively small. The ER data were obtained using scanning of 4x4 pixel squares with the scan period 1 pixel. Figure 4 represents reconstruction of images of five-pointed star without and with strong noise, utilizing only data of its ER with scanning squares. Figure 5 demonstrates reconstruction of hand-mask image noise free and strong noisy, using the similar ER data and rules. Note that Figures 4d and 5d demonstrate effective denoising capability of the algorithm (15), (16), (27).

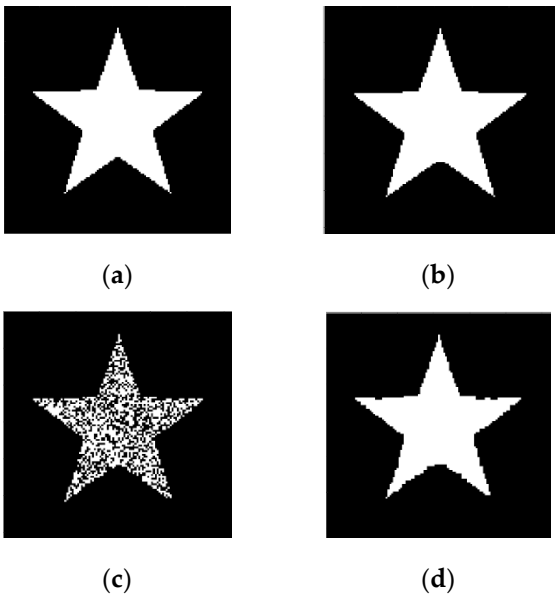

(**a**) (**b**)

(**c**) (**d**)

Figure 4. Results of reconstruction of five-pointed star based on qualitative data. (**a**) Original star; (**b**) Reconstructed star; (**c**) Original strong noisy star; (**d**) Reconstructed noisy star.

(**a**) (**b**)

Preprints (www.preprints.org) | NOT PEER-REVIEWED | Posted: 22 December 2022 doi:10.20944/preprints202212.0423.v1

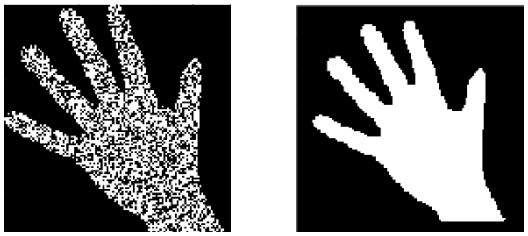

(**c**) (**d**)

Figure 5. Results of reconstruction of a hand-mask image based on qualitative data. (**a**) Original image; (**b**) Reconstructed image; (**c**) Original strong noisy image; (**d**) Reconstructed noisy image.

4.2. Reconstruction of Gray Scale Images

To be able to apply the developed reconstruction algorithm (15), (16), (27) to gray-scale images, it is necessary to add a new dimension to 2D spots corresponding to their intensity value. In order for this numerical coordinate to be consistent with the general spot ideology, we represent the intensity axes as a linear structure, chain of intersected spots (Figure 6).

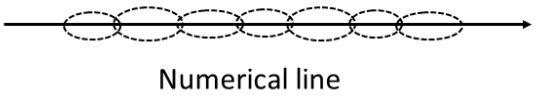

Figure 6. Representation of a numerical line as a chain of intersected spots.

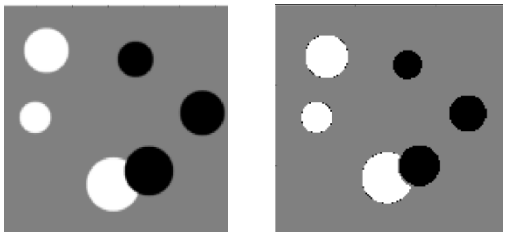

(**a**) (**b**)

Figure 7. Reconstruction of a circles image based on qualitative data. (**a**) Original image; (**b**) Reconstructed image.

For example, these spots can be numerical intervals, and hence we can split the gray-scale image into flat layers, corresponding to these intervals. Then one can reconstruct images in the layers independently and combine them again into the entire image. This approach was used for the image reconstruction demonstrated in Figures 7 – 10, where the intensity axes of images were divided into 10 layers.

(**a**) (**b**)

Figure 8. Reconstruction of Shepp-Logan image based on qualitative data. (**a**) Original image; (**b**) Reconstructed image.

Preprints (www.preprints.org) | NOT PEER-REVIEWED | Posted: 22 December 2022 doi:10.20944/preprints202212.0423.v1

As before, the ER data were obtained using a 4x4 pixel squares that were scanned in each of 10 layers, and their scan period was 1 pixel. Note that, Figures 9d, 10d, 10f also demonstrate noise reduction ability of the reconstruction algorithm (15), (16), (27).

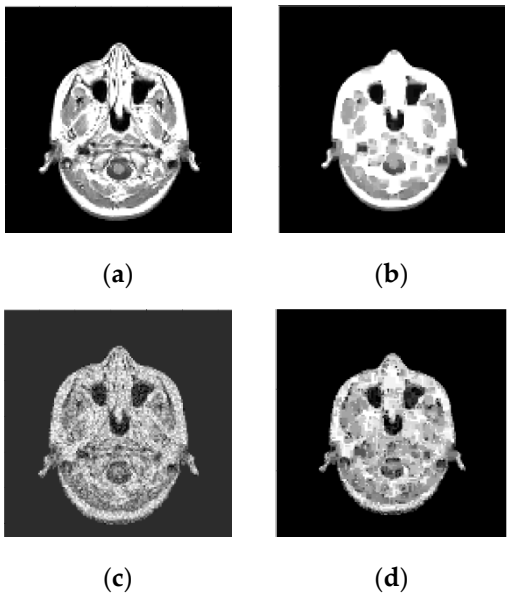

Figure 9. Results of reconstruction of MRI image based on qualitative data. (**a**) Original image; (**b**) Reconstructed image; (**c**) Original noisy image; (**d**) Reconstructed noisy image .

4.3. Inverse Radon Image Reconstruction

We used a MATLAB program to compare a conventional back-projection and a spot-based (31) algorithms for reconstruction of binary images, which used under-sampled parallel-beam sinograms for 6, 9 and 18 projection angles only. Figures 11, 12 show results of this comparison. The sinograms are calculated using Radon transform, but they imitate the real experimental sinograms of X-ray transmission through the body in CT system with parallel-beam geometry [3]. Note that typically a CT scanner collects projection signals in approximately 1° increments, and hence the simulated examples in Figures 11 and 12 are indeed highly under-sampled.

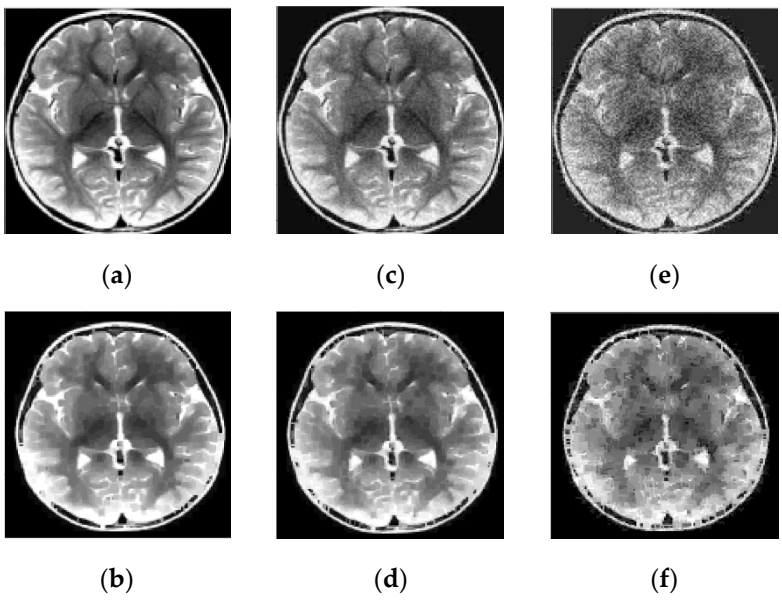

Preprints (www.preprints.org) | NOT PEER-REVIEWED | Posted: 22 December 2022 doi:10.20944/preprints202212.0423.v1

Figure 10. Results of reconstruction of MRI human brain image based on qualitative data. (**a**) Original image; (**b**) Reconstructed image; (**c**) Original low noise image; (**d**) Reconstructed low noise image; (**e**) Original noisy image; (**f**) Reconstructed noisy image.

Application of the back-projection algorithm with Hann filter is demonstrated in Figure 11 for two images of ellipse: nose-free (11a) and strong noisy (11e). It is clear that results of the noisy image reconstruction in Figure 11f, g, h demonstrate significant blurring for the reconstructed image.

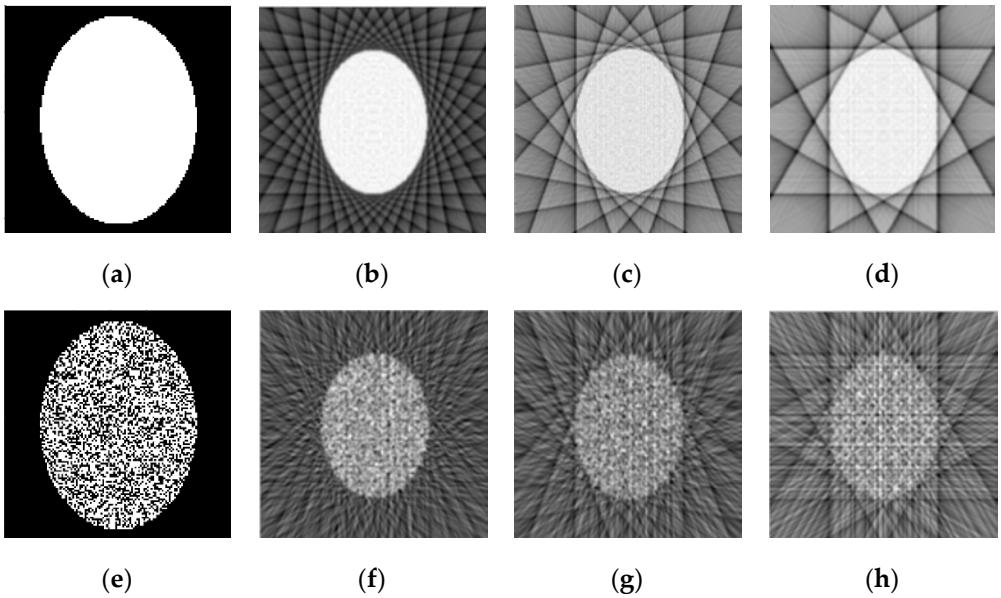

Figure 11. Examples of reconstruction of two ellipses, using their under-sampled parallel-beam sinograms by the back-projection algorithm with Hann filter. (**a**) Original ellipse; (**b**), (**c**), and (**d**) Reconstructed images for 18, 9 and 6 projection angles, correspondingly; (**e**) Original strong noisy ellipse; (**f**), (**g**), and (**h**) Reconstructed images for 18, 9 and 6 projection angles, correspondingly.

Figure 12 shows results of the same image reconstructions, using the spot-based algorithm (30), (31) with 5x5 pixels square and 1 pixel scan period. These results of the reconstruction demonstrate the fact that suggested algorithm allows to reconstruct unblurred images even for a small number of projection angles. Images in Figure 12f, g, and h also demonstrate strong denoising effect for the spot-based algorithm, in contrast to the back-projection algorithm.

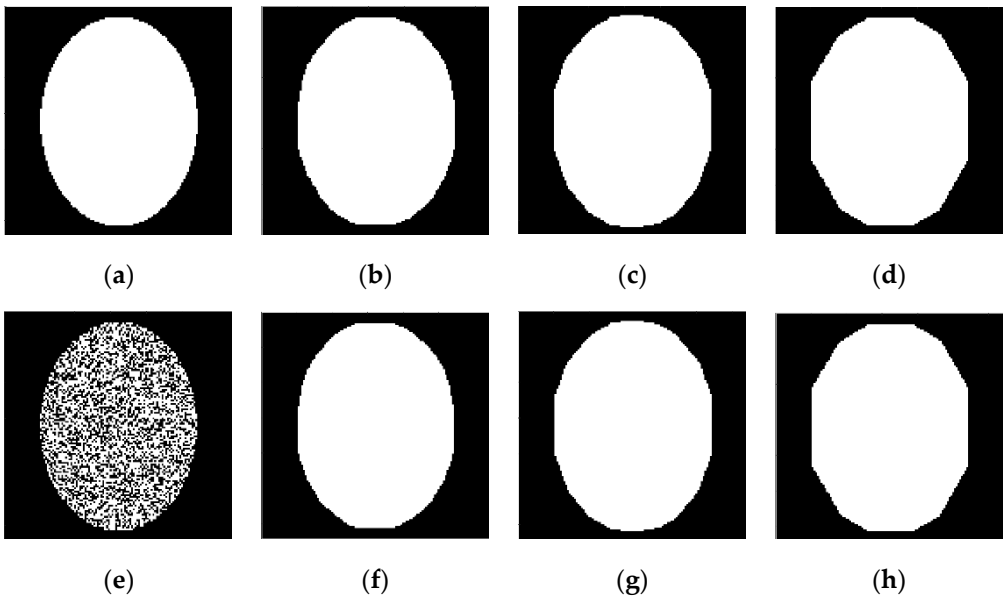

Preprints (www.preprints.org) | NOT PEER-REVIEWED | Posted: 22 December 2022 doi:10.20944/preprints202212.0423.v1

Figure 12. Reconstruction of two ellipses, using their different under-sampled sinograms. (**a**) Original ellipse; (**b**), (**c**), and (**d**) Reconstructed images for 18, 9 and 6 projection angles, correspondingly; (**e**) Original strong noisy ellipse; (**f**), (**g**), and (**h**) Reconstructed images for 18, 9 and 6 projection angles, correspondingly.

5. Discussion

In [27], the use of the apparatus of the spots model for creating neural networks of a new type is considered, in which each layer corresponds to an L4 matrix and L4 numbers are used instead of real numbers. Here, the L4 vectors play the role of input and output signals for each layer, and the L4 matrix of each layer, plays the role of the weight matrix. For example, equations (21) and (23) can be implemented using such a neural network, which consists of 4 and 3 layers, respectively. In addition, it is possible to create a neural network in the form of a neuromorphic electronic device built on solid-state elements such as field-effect transistors (FETs), FeFETs, or memristors [27].

The potential advantage of the proposed neural networks over conventional ones is, in particular, that the L4 matrix apparatus does not use real numbers with complex calculations during iterations in the backpropagation algorithm of learning by examples. Instead, equation (24) uses the inverse matrix product. Although the proposed algorithms are approximate, they are adequate to the fact that it is almost always impossible to obtain an exact solution to inverse problems due to the finite number of measured signals. In addition, the tasks of recognition and classification, in principle, do not belong to the class of tasks that require accurate calculations.

The reconstructed images in Figures 4, 5, 7–12 demonstrate a good denoising ability of the proposed algorithm. This property relates to the fact that a scanning squares of 4x4 or 5x5 pixels plays the role of a spatial filter and average the sampled data. However, the spatial resolution of the reconstructed image is determined by the scan period of 1 pixel. This can be explained using formulas (15) and (27), from which it follows that the resolution corresponds to the intersections size of 1x1 pixels.

An imaging algorithm using the spot-based inverse Radon tranform (equation (31) and Figure 12) illustrates the processing of qualitative data for solving by learning. Indeed, sampling figures are basis spots and also relates to training set, whereas the figure under test corresponds to the test example in the machine learning paradigm [29]. Finally, the reconstructed image, which is mapped on the basis of the intersections, corresponds to the solution of trained system.

As it was noted in the Introduction, we can draw a general conclusion about the ideological proximity of the models of spots and coarse sets [49-53], although they have a fundamental difference. In addition, there are several close concepts between the spot model and the rough set theory (see Table 2).

Table 2. Analogies between the concepts of rough sets and spots.

Concepts of the rough set theory	Concepts of the spots model
elements of the universe	atomic basis
granules	spots
attributes	basis of spots
attributes values	L4 numbers
boundary region	boundary
lower approximation	inner region
upper approximation	inner region + boundary

As it is shown in the Table 2, spots are similar to granules, which is also main concept in the granular computing (GC) research area [63–69]. Comparison of the spot and granule concepts in GC allows to conclude that both models are also very close in many aspects.

The suggested spots model can be used for the theory of qualitative geometry (QG). For this application, it is necessary to introduce new concepts that are low-level analogies of the notion in the geometry and topology, including line, surface, dimensionality,

 doi:10.20944/preprints202212.0423.v1

curvature of space, etc. Based on the CG, one can introduce the concept of a semantic information space, which is an analogue of an information system characterized by an information table and is used, for example, in the theory of rough sets [50,53].

6. Conclusions

This article is devoted to the description of the concept and the basis of the apparatus of new mathematical objects - spots, which are introduced to represent and process qualitative data. It can be used to model human mental images, perceptions and reasoning in AI. Also, this paper demonstrates another application of the developed apparatus – for solving inverse problems by the learning method.

The proposed model uses such qualitative information about spots as elementary relations between them, and introduces L4 logical numbers that encode these relations. Based on L4 numbers, the theory introduces L4 vectors and L4 matrices using the analogy with numerical matrix algebra. Although L4 numbers correspond to an elementary level of qualitative data, fusing of a large number of them allows you to extract a higher level information, including numerical.

Equations have been derived for reconstructing an image using only qualitative information about its elementary relations with a set of basis figures. A general scheme for solving inverse problems for L4 and numerical data is proposed, including a learning method for solving.

The introduced apparatus was tested by solving image reconstruction problems using only qualitative data of its elementary relations with the scan figures. The application of spot-based inverse Radon's algorithm for the reconstruction of a binary image was also demonstrated.

Further research in the field of the proposed theory involves the development of algorithms for solving various inverse problems, including inverse electromagnetic scattering. Another goal of the work is to design the neural networks based on the proposed spots model, where each layer corresponds to the L4 matrix.

Funding: The investigation was supported by the Program no. FFNN-2022-0019 of the Ministry of Science and Higher Education of Russia for Valiev Institute of Physics and Technology of RAS.

Acknowledgments: The author expresses deep appreciation to Lukichev V.F. and Rudenko K.V. for the support and discussion of this work.

Conflicts of Interest: The author declare no conflict of interest.

References

1. Ramm, A.G. *Inverse problems: mathematical and analytical techniques with applications to engineering,* Springer Science & Business Media: Berlin/Heidelberg, Germany 2006.
2. Devaney, A.J. *Mathematical foundations of imaging, tomography and wavefield inversion,* Cambridge University Press: Cambridge, UK, 2012.
3. Mudry, K.M.; Plonsey, R.; Bronzino, J.D. *Biomedical imaging,* CRC press: Boca Raton, Florida, USA, 2003.
4. Maisto, M.A.; Masoodi, M.; Pierri, R.; Solimene, R. Sensor Arrangement in Through-the Wall Radar Imaging. *IEEE Open Journal of Antennas and Propagation* **2022**, *3*, 333–341.
5. Chen, X. *Computational methods for electromagnetic inverse scattering,* John Wiley & Sons: Hoboken, N.J., USA, 2018.
6. Chandra,R.; Zhou, H.; Balasingham, I.; Narayanan, R.M. On the opportunities and challenges in microwave medical sensing and imaging. *IEEE Trans. Biomed. Eng.* **2015**, *62*, 1667–1682.
7. Simonov, N.; Kim, B.-R.; Lee, K.-J.; Jeon, S.-I.; Son, S.-H. Advanced fast 3D electromagnetic solver for microwave tomography imaging. *IEEE Trans. Med. Imag.* **2017**, *36*, 2160–2170.
8. O'Loughlin, D.; O'Halloran, M.; Moloney, B.M.; Glavin, M.; Jones, E.; Elahi, M.A. Microwave breast imaging: Clinical advances and remaining challenges. *IEEE Trans. Biomed. Eng.* **2018**, *65*, 2580–2590.
9. Shao, W.; McCollough, T. Advances in microwave near-field imaging: Prototypes, systems, and applications. *IEEE Microw. Mag.* **2020**, *21*, 94–119.
10. Simonov, N.; Son, S.H. Overcoming Insufficient Microwave Scattering Data in Microwave Tomographic Imaging. *IEEE Access* **2021**, *9*, 111231–111237. doi:10.1109/ACCESS.2021.3103414.
11. Li, K.; Tang, J. Chen, G.H. Statistical model-based iterative reconstruction (MBIR) in clinical CT systems: experimental assessment of noise performance. *Radiat. Imag. Phys.* **2014**, *41*, 041906. https://doi.org/10.1118/1.4867863.

12. Pickhardt, P.J.; Lubner, M.G.; Kim, D.H.; Tang, J.; Ruma, J.A.; del Rio, A.M.; Chen, G.H. Abdominal CT with model-based iterative reconstruction (MBIR): initial results of a prospective trial comparing ultralow-dose with standard-dose imaging. *AJR. American journal of roentgenology* 2012, *199*, 1266. doi/full/10.2214/AJR.12.9382
13. Fessler, J.A. Model-Based Image Reconstruction for MRI. *IEEE Signal Process. Mag.* **2010**, *27*, 81–89.
14. Wang, X.; Tan, Z.; Scholand, N.; Roeloffs, V.; Uecker, M. Physics-based reconstruction methods for magnetic resonance imaging. *Phil. Trans. R. Soc. A* **2021**, *379*, 20200196. https://doi.org/10.1098/rsta.2020.0196
15. McLeavy, C.M.; Chunara, M.H.; Gravell, R.J.; Rauf, A.; Cushnie, A.; Talbot, C.S.; Hawkins, R.M. The future of CT: deep learning reconstruction. *Clinical radiology* **2021**, *76*, 407-415.
16. Lee, D.; Lee, J.; Ko, J.; Yoon, J.; Ryu, K.; Nam, Y. Deep learning in MR image processing. *Investigative Magnetic Resonance Imaging* **2019**, *23*, 81–99.
17. Khoshdel, V.; Ashraf, A.; LoVetri, J. Enhancement of multimodal microwave-ultrasound breast imaging using a deep-learning technique. *Sensors* **2019**, *19*, 4050.
18. Wu, H.; Ren, X.; Guo, L.; Li, Z. A Non-Iterative Method Combined with Neural Network Embedded in Physical Model to Solve the Imaging of Electromagnetic Inverse Scattering Problem. *Electronics* **2021**, *10*, 3104.
19. Gao, F.; Huang, T.; Sun, J.; Wang, J.; Hussain, A.; Yang, E. A new algorithm for SAR image target recognition based on an improved deep convolutional neural network. *Cognitive Computation* **2019**, *11*, 809–824.
20. Chen, X.; Wei, Z.; Li, M.; Rocca, P. A review of deep learning approaches for inverse scattering problems (invited review). *Progress In Electromagnetics Research* **2020**, *167*, 67–81.
21. Zhu, X.; Montazeri, S.; Ali, M.; Hua, Y.; Wang, Y.; Mou, L.; Shi, Y.; Xu, F.; Bamler, R. Deep learning meets SAR: concepts, models, pitfalls, and perspectives. *IEEE Geoscience and Remote Sensing Magazine (GRSM)* **2021**, *9*,143–172. https://doi.org/10.1109/MGRS.2020.3046356
22. Alshammari, M.M.; Almuhanna, A.; Alhiyafi, J. Mammography Image-Based Diagnosis of Breast Cancer Using Machine Learning: A Pilot Study. *Sensors* **2022**, *22*, 203. https://doi.org/10.3390/s22010203
23. Fayaz, M.; Torokeldiev, N.; Turdumamatov, S.; Qureshi, M.S.; Qureshi, M.B.; Gwak, J. An Efficient Methodology for Brain MRI Classification Based on DWT and Convolutional Neural Network. Sensors **2021**, *21*, 7480. https://doi.org/10.3390/s21227480
24. Awan, M.J.; Rahim, M.S.M.; Salim, N.; Rehman, A.; Garcia-Zapirain, B. Automated Knee MR Images Segmentation of Anterior Cruciate Ligament Tears. Sensors **2022**, *22*, 1552. https://doi.org/10.3390/s22041552
25. Simons, T.; Lee, D.J. A review of binarized neural networks. *Electronics* **2019**, *8*, 661.
26. Aggarwal, C.C. Neural networks and deep learning. Springer: Cham, Switzerland, 2018; Volume 10, 978-3. https://doi.org/10.1007/978-3-319-94463-0
27. Simonov, N.A. Spots Concept for Problems of Artificial Intelligence and Algorithms of Neuromorphic Systems. *Russian Microelectronics* **2020**, *49*, 431–444. https://doi.org/10.1134/S106373972005008X
28. Simonov, N. The Spot Model for Representation and Processing of Qualitative Data and Semantic Information. In Proceedings of Selected Contributions to the Russian Advances in Artificial Intelligence Track at RCAI 2021, Taganrog, Russia, October 11-16, 2021, CEUR-WS, US, 16-Dec-2021, pp. 55-69. urn:nbn:de:0074-3044-4
29. Goodfellow, I.; Bengio, Y.; Courville, A. *Deep Learning*, MIT Press: Cambridge, UK, 2016.
30. Whitehead, A.N. Process and reality: An essay in cosmology. Cambridge University Press: Cambridge, UK, 1929.
31. Clarke, B.L. A calculus of individuals based on connection. *Notre Dame Journal of Formal Logic* **1981**, *22*, 204–218.
32. Asher, N.; Vieu, L. Toward a geometry of common sense: A semantics and a complete axiomatization of mereotopology. In Proceedings of IJCAI'95-ATAL Workshop, Montreal, Canada, August 19-20, 1995, pp. 846-852.
33. Stell, J.G. *Mereotopology and computational representations of the body. Computational Culture* **2017**, *6*.
34. Cohn, A.G.; Bennett, B.; Gooday, J.; Gotts N. Qualitative spatial representation and reasoning with the Region Connection Calculus. *GeoInformatica* **1997**, *1*, 275–316.
35. Cohn, A.G.; Renz, J. Qualitative Spatial Representation and Reasoning. In *Handbook of Knowledge Representation*; van Harmelen, F., Lifschitz, V., Porter, B., Eds.; Elsevier B.V.: Amsterdam, Netherlands, 2008; Ch. 13, 551 – 596. https://doi.org/10.1016/S1574-6526(07)03013-1
36. Cohn, A.G.; Gotts, N.M. A mereological approach to representing spatial vagueness. In Proceedings of 5th Conference Principles of Knowledge Representation and Reasoning, Morgan Kaufmann: Burlington, US, 1996; pp. 230–241.
37. Galton, A. The mereotopology of discrete space. In Proceedings of International Conference COSIT'99, Stade, Germany, August 25-29, 1999; pp. 251–266.
38. Galton, A. Discrete mereotopology. In *Mereology and the Sciences*; Calosi, C., Graziani; P. Eds.; In *Synthese Library (Studies in Epistemology, Logic, Methodology, and Philosophy of Science);* Springer: Cham, Switzerland, 2014; Volume 371, pp. 293–321.
39. Balbiani, P.; Gencer, C. Finitariness of elementary unification in Boolean Region Connection Calculus. In *International Symposium on Frontiers of Combining Systems;* Springer: Cham, Switzerland, 2017; pp. 281–297.
40. Izadi, A.; Stock, K.M.; Guesgen, H.W. Multidimensional Region Connection Calculus. In Proceedings of 30th International Workshop on Qualitative Reasoning, Melbourne, Australia, August 21, 2017.
41. Davari S.; Ghadiri N. Fuzzy region connection calculus and its application in fuzzy spatial skyline queries. In *Intelligent Computing-Proceedings of the Computing Conference;* Arai, K., Bhatia, R., Kapoor, S. Eds.; Springer: Cham, Switzerland, 2019; Volume 997, pp. 659-677.

42. Bennett, B. Spatial reasoning with propositional logics. In *Proceedings of the 4th International Conference on Principles on Knowledge Representation and Reasoning (KR-94)*; Doyle, J., Sandewall, E., Torasso, P. Eds.; Morgan Kaufmann: Bonn, Germany, 1994; pp. 165–176.
43. Jonsson, P.; Drakengren, Th. A complete classification of tractability in RCC-5. *Journal of Artificial Intelligence Research* **1997**, *6*, 211–221.
44. Egenhofer, M.J.; Franzosa, R. Point-set topological spatial relations. *International Journal of Geographical Information Systems* **1991**, *5*, 161–174.
45. Egenhofer, M.J.; Herring, J.R. Categorizing binary topological relations between regions, lines and points in geographic databases. Technical Report, Department of Surveying Engineering, University of Maine, 1991.
46. Clementini, E.; Di Felice, P. Approximate topological relations. *International journal of approximate reasoning* **1997**, *16*, 173–204.
47. Stell, J.G. Part and complement: fundamental concepts in spatial relations. *Annals of Mathematics and Artificial Intelligence* **2004**, *41*, 1–17.
48. Butenkov, S.A.; Krivsha, V.V.; Krivsha, N.S. The Use of the Mathematical Apparatus of Spatial Granulation in The Problems of Perception and Image Recognition. *Recognition and Perception of Images: Fundamentals and Applications* **2021**, 221–259. https://doi.org/10.1002/9781119751991.ch7
49. Pawlak, Z. Rough sets. *International Journal of Computer and Information Sciences* **1982**, *11*, 341–356.
50. Pawlak, Z.: Rough set theory and its applications to data analysis. *Cybernetics and Systems* **1998**, *29*, 661–688. https://doi.org/10.1080/019697298125470.
51. Suraj, Z. An Introduction to Rough Set Theory and Its Applications: A Tutorial. In Proceedings of 1st International Computer Engineering Conference (ICENCO') New Technologies for the Information Society, Cairo, Egypt, December 27-30, 2004; pp. 1–39.
52. *Rough Sets: Selected Methods and Applications in Management and Engineering*; Peters, G., Lingras, P., Slezak, D., Yao, Y.Y. Eds.; Springer: London, UK, 2012.
53. Yao, Y.Y. Rough set approximations: A concept analysis point of view. In *Computational Intelligence;* Ishibuchi, H. Ed.; Volume I, *Encyclopedia of Life Support Systems,* 2015; UNESCO-EOLSS; pp. 282–296.
54. Skowron, A.; Dutta, S. Rough sets: past, present, and future. *Natural Computing* **2018**, *17*, 855–876. https://doi.org/10.1007/s11047-018-9700-3.
55. Sun, L.; Wang, L.; Xu J.; Zhang, Sh. A neighborhood rough sets-based attribute reduction method using Lebesgue and entropy measures. *Entropy* **2019**, *21*, 138. https://doi.org/10.3390/e21020138.
56. Slim, H.; Nadeau S. A mixed rough sets/fuzzy logic approach for modelling systemic performance variability with FRAM. *Sustainability* **2020**, *12*, 1918. https://doi.org/10.3390/su12051918.
57. Wille, R. Restructuring lattice theory: An approach based on hierarchies of concepts. In *Ordered Sets;* Rival, I. Ed.; Reidel: Dordrecht, Netherland, 1982; pp. 445-470.
58. Ganter, B.; Wille, R. *Formal Concept Analysis: Mathematical Foundations*; Springer: New York, US, 1999.
59. Wille, R. Formal Concept Analysis as Mathematical Theory of Concepts and Concept Hierarchies. In *Formal Concept Analysis, LNAI 3626*; Ganter, B. et al. Eds.; Springer-Verlag: Berlin, Heidelberg, 2005; pp. 1–33.
60. Zadeh, L.A. Fuzzy sets. *Inf. Control* **1965**, *8*, 338-35.
61. Buckley, J.J.; Eslami, E. Fuzzy plane geometry I: points and lines. *Fuzzy Sets Syst* **1997**, *86*, 179–187.
62. Buckley, J.J.; Eslami, E. Fuzzy plane geometry II: circles and polygons. *Fuzzy Sets Syst.* **1997**, *87*, 79–85.
63. Zadeh, L.A. Towards a theory of fuzzy information granulation and its centrality in human reasoning and fuzzy logic. *Fuzzy Sets Syst.* **1997**, *19*, 111-127.
64. Yao, J.T. A Ten-year Review of Granular Computing. In *Proc. IEEE Int. Conf. on Granular Computing*, Silicon Valley, USA, Nov 2–5, 2007; pp. 734–739.
65. Lin, T.Y. Data mining: granular computing approach. In Proceedings of the Pacific-Asia Conference on Knowledge Discovery and Data Mining, 1999; Springer: Berlin, Heidelberg, Germany; pp. 24–33.
66. Yao, Y.Y. Information granulation and rough set approximation. *International Journal of Intelligent Systems* **2001**, *16*, 87–104.
67. Nguyen, S.H.; Skowron, A.; Stepaniuk, J. Granular computing: a rough set approach. *Comput. Intell.* **2001**, *17*, 514–544.
68. Yao, J.T.; Vasilakos, A.V.; Pedrycz, W. Granular Computing: Perspectives and Challenges. *IEEE Trans. on Cybernetics* **2013**, *43*, 1977–1989.
69. Skowron, A.; Jankowski, A.; Dutta, S. Interactive granular computing. *Granul. Comput.* **2016**, *1*, 95–113.
70. Diestel, R. *Graph Theory*, 3rd ed.; Springer-Verlag: Berlin, New York, 2005**.**
71. Klette, R.; Rosenfeld, A. *Digital geometry: Geometric methods for digital picture analysis*. Elsevier, Morgan Kaufmann Publishers: San Francisco, US, 2004; Ch. 4,5.
72. Rubinov, M.; Sporns, O. Complex network measures of brain connectivity: uses and interpretations. *NeuroImage*, **2010**, *52*, 1059–1069.
73. Cao, S.; Lu, W.; and Xu, Q. Deep neural networks for learning graph representations. In Proceedings of the 30th AAAI Conference on Artificial Intelligence, Phoenix, Arizona, US, February 12-17, 2016; pp. 1145–1152.
74. Defferrard, M.; Bresson, X.; Vandergheynst, P. Convolutional neural networks on graphs with fast localized spectral filtering. In Proceedings of the 30th Conf. on Neural Information Processing Systems (NIPS 2016), Barcelona, Spain, December 5–10, 2016; pp. 3844–3852.

 doi:10.20944/preprints202212.0423.v1

75. Cui, P.; Wang, X.; Pei, J.; Zhu, W. A survey on network embedding. *IEEE Trans. on Knowledge and Data Engineering* **2019**, *31*, 833 – 852.
76. Bordes, A.; Usunier, N.; Garcia-Dur´an, A.; Weston, J.; Yakhnenko, O. Translating embeddings for modeling multi-relational data. In *Advances in Neural Information Processing Systems 26*; Burges, C.J.C., Bottou, L., Welling, M., Ghahramani, Z. Eds.; Curran Associates, Inc.: NY, US, 2018, pp. 2787–2795.
77. Wang, Zh.; Zhang, J.; Feng, J.; and Chen, Zh. Knowledge graph embedding by translating on hyperplanes. In Proc. 28th AAAI Conference on Artificial Intelligence,
78. Québec City, Québec, Canada, July 27–31, 2014; pp. 1112–1119.